CHARACTERISTIC TIMES OF GRADUAL SOLAR ENERGETIC PARTICLE EVENTS AND THEIR DEPENDENCE ON ASSOCIATED CORONAL MASS EJECTION PROPERTIES

S. W. KAHLER

Air Force Research Laboratory, Space Vehicles Directorate, 29 Randolph Road, Hanscom AFB, MA 01731;
stephen.kahler@hanscom.af.mil
Received 2004 July 5; accepted 2005 April 7

ABSTRACT

We use 20 MeV proton intensities from the EPACT instrument on *Wind* and coronal mass ejections (CMEs) from the LASCO coronagraph on *SOHO* observed during 1998–2002 to statistically determine three characteristic times of gradual solar energetic particle (SEP) events as functions of solar source longitude: (1) T_O, the time from associated CME launch to SEP onset at 1 AU, (2) T_R, the rise time from SEP onset to the time when the SEP intensity is a factor of 2 below peak intensity, and (3) T_D, the duration over which the SEP intensity is within a factor of 2 of the peak intensity. Those SEP event times are compared with associated CME speeds, accelerations, and widths to determine whether and how the SEP event times may depend on the formation and dynamics of coronal/interplanetary shocks driven by the CMEs. Solar source longitudinal variations are clearly present in the SEP times, but T_R and T_D are significantly correlated with CME speeds only for SEP events in the best-connected longitude range. No significant correlations between the SEP times and CME accelerations are found except for T_D in one longitude range, but there is a weak correlation of T_R and T_D with CME widths. We also find no correlation of any SEP times with the solar wind O^{+7}/O^{+6} values, suggesting no dependence on solar wind stream type. The SEP times of the small subset of events occurring in interplanetary CMEs may be slightly shorter than those of all events.

Subject headings: solar wind — Sun: coronal mass ejections (CMEs) — Sun: particle emission

Online material: machine-readable table

1. INTRODUCTION

1.1. *Timescales of SEP Events*

The peak intensities (Kahler 2001), energy spectra (Reames 1999), and elemental abundances (Tylka 2001) of gradual solar energetic ($E \geq 10$ MeV) particle (SEP) events are now understood to result primarily, if not exclusively, from first-order Fermi acceleration by coronal/interplanetary shocks driven by coronal mass ejections (CMEs). There remain major questions, such as the shock seed particle populations (Mewaldt et al. 2003; Kahler 2004), the role of shock normals (Tylka et al. 2005), and the effects of variations in the preshock ambient coronal and interplanetary conditions (Gopalswamy et al. 2003a, 2003b), but increasingly detailed modeling of the evolving shock properties, wave-particle interactions, and particle transport has reproduced major features of the gradual SEP events. Ng et al. (2003) have extended their earlier model (Ng et al. 1999) by including more physical processes, and Rice et al. (2003) significantly extended the earlier dynamical shell model (Zank et al. 2000), with the intent to use the spectrum of particles escaping upstream of the shock as the input to their recent upstream transport model (Li et al. 2003). These models can be tested for variations in elemental abundances and energy spectra (Tylka et al. 2005), but we still need a statistical description of the parameters characterizing SEP intensity-time profiles at 1 AU, which the models (Ng et al. 2003; Li et al. 2003) are now producing.

The first large statistical study of $E > 20$ MeV SEP events was probably that of van Hollebeke et al. (1975). Using 185 20 MeV $< E <$ 80 MeV SEP events from the *Interplanetary Monitoring Platform* (*IMP*) spacecraft, they focused on the early phases of SEP events and plotted times ΔT, from event onsets to maxima, as a function of solar source longitude. The time ΔT reached a minimum value of about 2.5 hr around W50° and increased for larger magnetic angular separations between the

Earth and the solar source longitude. Cane et al. (1988) surveyed a larger sample of 235 SEP events and plotted as a function of solar source longitude the delay times from associated Hα flare maxima to peak SEP intensities, some of which were peaks at 1 AU shock passages. In each of three proton energy ranges spanning ~1–100 MeV, those plots showed a pattern of delay times increasing from W90° to E90° source longitudes. A similar result was found for 112 $E > 10$ MeV proton events by Balch (1999).

The decay phases of gradual SEP events are characterized by a spatial and temporal invariance of the energy spectra, whose onset is ordered by the location of the observer relative to the interplanetary shock (Reames et al. 1996, 1997). Statistical analyses of $E > 4$ MeV proton event decay phases show a tendency for event decay times to decrease with higher shock speeds and with steeper energy spectra (Daibog et al. 2003), supporting the interpretation of adiabatic deceleration of SEPs quasi-trapped behind large-scale expanding shocks (Reames et al. 1996).

1.2. *CMEs and SEP Timescales*

Since CMEs are the drivers of shocks that accelerate SEPs, we might expect that the characteristics of the SEP intensity-time profiles observed at 1 AU are determined by properties of the associated CMEs. For example, faster CMEs may drive shocks for longer periods of time, resulting in SEP events of longer duration or rise times, as may be the case with $E > 300$ keV solar electrons (Stolpovskii et al. 1998).

Accelerations of CMEs have been the focus of considerable work since Sheeley et al. (1999) described two classes of CME speed profiles observed in the range 2–30 $R_\odot$, those gradually accelerating to 400–600 km s^{-1} and those with nearly uniform speeds typically in excess of 750 km s^{-1}. The second class are candidate drivers of interplanetary shocks and hence important for SEP events (Kahler 2001). Moon et al. (2002) found that the second class are more likely associated with flares and show

decelerations slightly increasing with speeds. The consensus (Zhang et al. 2001; Shanmugaraju et al. 2003; Gallagher et al. 2003) is that the speeds of fast CMEs are initially slow (<100 km s^{-1}) below $2\,R_{\odot}$ but then accelerate rapidly for several minutes or tens of minutes during the flare rise phases and move with nearly uniform speeds above $\sim4\,R_{\odot}$. Kocharov et al. (2001) selected CMEs with final speeds of 300–800 km s^{-1}, compared one group of high accelerations with another group of low accelerations and found that all SEP events of their study were associated with CMEs of high accelerations. As discussed by Kahler (2003), their study was based on an invalid comparison between accelerations in the 2–$32\,R_{\odot}$ field of view for one group and accelerations below that field of view for the other group. However, the importance, if any, of CME accelerations in the production of SEP events is still an open question.

CME widths may be an important factor for the temporal characteristics of gradual SEP events. We might expect that all CMEs of sufficient speed will drive shocks that can accelerate SEPs, but Kahler & Reames (2003) found that no fast ($v_{\mathrm{CME}} > 900$ km s^{-1}) CMEs with angular widths $W \leq 60^{\circ}$ were associated with gradual SEP events. Gopalswamy et al. (2001) found that CMEs associated with decameter-hectometric wavelength type II radio bursts, a strong signature of SEP events (Cliver et al. 2004) were significantly wider (102° vs. 66°) than the fast ($v_{\mathrm{CME}} > 900$ km s^{-1}) CMEs without those radio bursts. The shock structure should be a result of the interaction of the CME geometry with the ambient medium. LASCO observations of streamer deflections (Sheeley et al. 2000) and bow-shaped density enhancements (Vourlidas et al. 2003) at the flanks of fast CMEs suggest shocks traveling away from the CMEs with a range of angles between the magnetic fields and the shock normals. Tylka et al. (2005) have argued that SEP populations accelerated at quasi-perpendicular and at quasi-parallel shocks should show distinct differences, including longer event durations for SEPs from quasi-parallel shocks due to the longer propagation times of the shocks along given field lines. Although we cannot directly observe the characteristics of the CME-driven shocks, we might expect that broader CMEs would be more likely to produce parallel shocks and hence longer characteristic times for associated SEP events. Further, we might expect SEPs predominately from parallel (perpendicular) shocks when the associated CMEs are magnetically well (poorly) connected to Earth (see Fig. 4 of Kahler 2004). As the shock progresses outward through the interplanetary medium, the Earth-shock magnetic connection point moves from west to east, changing the angle between the shock normal and the interplanetary field direction (see Fig. 3.4 of Reames 1999).

SEP intensity time profiles may also be modified in various ways by large-scale interplanetary structures. Richardson & Cane (1996) found that the SEP flow directions at event onsets were highly variable inside solar ejecta but nearly always along Parker spiral field lines when the spacecraft was outside ejecta. Their results inside ejecta were consistent with the presence of looped field lines rooted to the Sun, with particles arriving from east or west of the Sun. Magnetic clouds (MCs) may facilitate rapid propagation of SEPs to 1 AU, as in the case of the 1998 May 2 SEP event (Torsti et al. 2004), or may serve as confining barriers to the SEPs, as in the 2000 July 14 SEP event (Kallenrode & Cliver 2001; Bieber et al. 2002). On magnetic fields draping nearby CMEs, the durations of SEP events can be extended due to the diminished focusing lengths of those fields (Tan et al. 1992; Kallenrode 2002). SEP profiles resulting from the interaction of two or more fast CMEs close together in space and time (Kahler 1993) may also appear considerably modified from those of individual SEP events.

CMEs have now been routinely observed with the Large Angle Spectroscopic Coronagraph (LASCO; Brueckner et al. 1995) on the *SOHO* spacecraft for over 8 yr, and statistical properties of LASCO CMEs have been summarized by St. Cyr et al. (2000) and by Yashiro et al. (2004). With the consensus that gradual SEP events result from CME-driven shock acceleration and with recent modeling generating SEP intensity-time profiles, it is now appropriate to examine SEP event time parameters, first simply to characterize them, and second to look for any systematic relationships between them and CME parameters.

We note that various authors have argued for alternative SEP injection scenarios based on flares (Cane & Erickson 2003) or additional flare/coronal phases of SEP injections, deduced from deviations from simple rise-and-fall profiles of some SEP events (Vashenyuk et al. 1994; Torsti et al. 1996; Klein et al. 1999; Miroshnichenko et al. 2000, Laitinen et al. 2000; Klein & Trottet 2001) or from temporal variations in SEP spectra (Torsti et al. 1999a, 1999b, 2001; Kocharov et al. 1999). We cannot rule out these scenarios for some SEP events, but arguments against injections from sources other than CME-driven shocks have been made (Kahler et al. 2000; Tylka et al. 2005), and here we assume that gradual SEP events are the products solely of injections from CME-driven shocks.

2. DATA ANALYSIS

2.1. *Event Selection and SEP Profile Time Parameters*

SEP intensity-time plots have traditionally used linear time axes, but logarithmic time axes were recently introduced for some SEP event analyses (Kocharov et al. 1999; Torsti et al. 2001). These plots, known as lognormal, describe well the distributions of a broad range of populations and have been applied to time series of the geomagnetic storm parameter *Dst* (Campbell 1996). Yago & Kamide (2003) have shown that the lognormal plot is a good fit for *Dst* for many storms, allowing predictions of the recovery phases to be made. For SEP events the lognormal fits expand the relatively short rise phases and compress the longer decay phases so that the resulting profile approaches a normal distribution. These plots may prove useful for determining SEP injection and propagation characteristics, but in this work we continue the use of linear time axes and timescales.

We compiled a list of $E = 20$ MeV SEP events observed from 1998 through 2002 with the Energetic Particles: Acceleration, Composition, and Transport (EPACT; von Rosenvinge et al. 1995) experiment on the *Wind* spacecraft that could confidently be temporally associated with LASCO CMEs listed in the CME catalog.[1] The ratio of the peak 20 MeV SEP intensity to the preevent background also had to be at least 2 to obtain good SEP event profiles. Only CMEs associated with chromospheric or coronal solar source regions, determined from Hα flare reports and from EUV Imaging Telescope (EIT) and *Yohkoh* Soft X-Ray Telescope (SXT) movies, were used in the present analysis. No attempt was made to separate impulsive and gradual SEP events. The events of 2000 May 1, 2001 March 10, and 2002 February 20 are probably impulsive SEP events (Kahler 2003).

The dates and projected $1\,R_{\odot}$ launch times of the CMEs associated with the 144 selected SEP events are given in the first two columns of Table 1. In addition, each CME speed and acceleration, taken from the LASCO CME catalog, had to be based on a minimum of three data points; those parameters are given in the third and fourth columns of the table. The fifth and sixth columns give the reported CME angular widths and the

---

[1] See http://cdaw.gsfc.nasa.gov/CME_list.

TABLE 1
PROPERTIES OF CMEs AND ASSOCIATED SEP EVENTS

Date CME (1)	Launch (UT) (2)	v_{CME} (km s^{-1}) (3)	Acceleration (m s^{-2}) (4)	W (deg) (5)	Solar Location[a] (6)	T_O (hr) (7)	T_R (hr) (8)	½ Peak[b] (UT) (9)	T_D (hr) (10)	20 MeV Peak[c] (11)	O^{+7}/O^{+6} (12)
					1998						
Jan 26............	22:05	399	1.5	66	S17W55	2.4	2.5	Jan 27 3:00	5.0	0.008	...
Apr 20..........	9:55	1863	43.5	165	S43W90	1.6	12.5	24:00	36.0	30	0.5
Apr 29...........	16:30	1374	−44.8	360	S18E20	4.5	14.0	Apr 30 11:00	41.5	0.05	0.6
May 2............	13:20	938	−28.8	360	S15W15	1.2	2.0	16:30	8.5	2	0.7
May 6...........	8:00	1099	24.5	190	S11W65	0.5	1.0	9:30	1.0	4	0.6
May 9...........	3:25	2331	−140.5	178	S11W90	1.1	5.0	9:30	18.5	0.3	0.12
May 27.........	13:05	878	−3.7	268	N18W58	1.9	1.0	16:00	11.0	0.002	0.5
May 30.........	22:10	594	−10.3	63	bSWL	3.8	6.0	May 31 8:00	8.5	0.003	0.13
Jun 4.............	1:45	1802	−6.5	360	bNWL	8.7	8.5	19:00	17.0	0.01	0.17
Jun 16...........	18:00	1484	−74.7	281	S17W90	2.5	8.5	Jun 17 5:00	40.0	0.03	...
Nov 5	20:10	1118	−24.0	360	N22W18	1.8	11.0	Nov 6 9:00	6.0	0.03	0.25
Nov 24	2:10	1798	−12.5	360	S30W90	0.8	4.0	7:00	17.0	0.02	0.15
					1999						
Apr 24	13:02	1495	37.1	360	bWL	2.0	3.0	18:00	12.0	0.3	0.25
May 3...........	5:50	1584	15.8	360	N15E32	12.7	11.5	May 4 6:00	33.0	0.02	0.14
May 9...........	17:15	615	−3.0	172	N26W90	1.3	1.0	19:30	4.5	0.04	0.2
May 27.........	10:40	1691	−33.5	360	bWL	0.7	1.5	12:30	6.5	0.15	0.2
Jun 1.............	18:33	1772	1.8	360	bNWL	2.0	8.0	Jun 2 4:30	30.5	0.8	0.45
Jun 4.............	6:45	2230	−158.8	150	N17W69	1.7	1.5	10:00	18.0	0.8	0.25
Jun 11...........	0:20	719	−38.2	101	bSWL	0.7	1.0	2:00	2.5	0.07	0.4
Jun 27...........	8:15	903	−27.7	86	N23W25	3.3	2.0	13:30	9.0	0.004	0.2
Jun 29...........	6:58	634	1.1	360	N18E04	5.0	27.0	Jun 30 15:00	37.0	0.002	0.26
Jul 25............	13:12	1389	−16.4	360	N38W81	8.3	4.5	Jul 26 2:00	29.0	0.0015	0.15
Aug 28	17:40	462	1.1	245	S26W14	3.3	1.0	22:00	12.5	0.001	0.2
Sep 14	7:15	761	21.0	122	NWL	0.0	1.0	7:00	17.0	0.0025	0.35
Oct 14	8:43	1250	−21.2	360	N11E32	10.3	9.0	Oct 15 5:00	46.0	0.0015	0.09
Dec 28..........	0:25	672	−14.5	82	N20W56	2.6	2.0	5:00	12.0	0.004	1
					2000						
Jan 18...........	17:10	739	−7.1	360	S19E11	2.8	2.0	22:00	42.0	0.02	0.3
Feb 12	4:05	1107	−8.3	360	N26W23	2.4	1.5	8:00	6.0	0.04	0.45
Feb 17	20:05	728	−22.9	360	S29E07	1.9	2.0	Feb 18 0:00	...	0.02	...
Feb 18	9:05	890	−9.6	118	bNWL	0.9	0.5	10:30	2.5	0.4	0.6
Mar 2............	8:05	776	0.8	62	S14W52	1.9	2.0	12:00	8.0	0.01	0.2
Mar 3............	2:05	841	−1.0	98	S15W60	1.4	0.5	4:00	3.0	0.01	0.2
Apr 4............	14:53	1188	12.8	360	N16W66	1.6	5.5	22:00	15.5	0.4	0.4
Apr 23	12:08	1187	−48.5	360	bNWL	3.4	4.0	19:30	19.5	0.015	0.2
Apr 27	14:00	1110	−10.9	138	N32W90	2.5	0.5	17:00	10.0	0.003	0.5
May 1	10:13	1360	−62.6	54	W54	0.8	0.5	11:30	2.5	0.002	0.4
May 4...........	10:53	1404	28.2	170	S17W90	1.1	4.0	16:00	22.0	0.003	0.7
May 5...........	15:18	1594	−103.4	360	SW90	4.7	10.0	May 6 6:00	32.0	0.005	0.35
May 10.........	19:10	641	−15.5	205	N14E20	9.3	3.0	May 11 7:30	24.5	0.0015	0.45
May 15.........	15:45	1212	−20.5	165	S24W67	3.7	2.5	21:30	8.5	0.015	0.65
Jun 2.............	20:30	731	19.9	112	N16E60	9.0	11.0	Jun 4 16:30	30.5	0.0008	0.4
Jun 6.............	15:20	1119	1.5	360	N33E25	4.2	21.5	Jun 7 17:00	16.0	0.4	0.9
Jun 10...........	16:45	1108	−21.2	360	N22W38	0.7	0.5	18:00	7.0	1.3	0.7
Jun 15...........	19:25	1081	−16.7	116	N20W65	1.6	1.0	22:00	15.5	0.0013	0.25
Jun 17...........	2:40	857	16.4	133	N22W72	2.8	0.5	6:00	7.5	0.006	0.2
Jun 18...........	1:40	629	−1.2	132	N23W85	0.8	1.0	3:30	6.5	0.04	0.25
Jun 23...........	13:50	847	−23.3	198	N26W72	1.2	1.5	16:30	3.5	0.015	0.3
Jun 25...........	7:42	1617	−17.5	165	N16W55	3.8	2.5	14:00	17.5	0.03	1
Jun 28...........	18:38	1198	−21.9	134	N20W90	1.9	1.0	21:30	8.5	0.002	0.25
Jul 10............	21:20	1352	35.0	289	N18E49	1.2	4.5	Jul 11 3:00	10.5	0.007	0.7
Jul 11............	12:32	1078	−42.9	360	N18E27	2.5	1.0	16:00	32.0	0.005	1.1
Jul 14............	10:25	1674	−96.1	360	N22W07	1.1	1.5	13:00	26.0	120	0.17
Jul 22............	11:20	1230	−12.4	229	N14W56	1.2	1.0	13:30	9.5	0.3	0.6
Aug 12	9:38	662	−6.7	168	bWL	0.9	1.5	12:00	2.0	0.03	0.46
Aug 12	14:03	876	10.6	161	N13W46	2.0	1.0	17:00	12.0	0.005	1.2
Aug 13	6:00	883	20.4	154	bWL	11.0	6.5	23:30	20.5	0.007	2.1

1016

TABLE 1—*Continued*

Date CME (1)	Launch (UT) (2)	v_{CME} (km s^{-1}) (3)	Acceleration (m s^{-2}) (4)	W (deg) (5)	Solar Location[a] (6)	T_O (hr) (7)	T_R (hr) (8)	$\frac{1}{2}$ Peak[b] (UT) (9)	T_D (hr) (10)	20 MeV Peak[e] (11)	O^{+7}/O^{+6} (12)
Sep 9	7:40	554	−13.4	180	N07W67	3.3	1.0	12:00	9.0	0.008	0.85
Sep 12	11:45	1550	58.2	360	S17W09	1.7	5.5	19:00	26.0	2	0.3
Sep 19	8:10	766	10.4	76	N14W46	4.8	2.0	15:00	18.0	0.013	0.45
Oct 9	23:00	798	−9.8	360	N01W14	8.0	7.0	14:00	43.0	0.005	0.43
Oct 16	6:50	1336	9.9	360	bWL	0.7	3.5	11:00	14.5	0.4	0.12
Oct 25	8:55	770	17.4	360	W50	3.6	5.0	17:30	16.5	0.25	0.22
Nov 8	22:48	1738	69.9	170	N10W77	0.7	3.5	Nov 9 3:00	15.0	150	1.2
Nov 24	5:08	994	72.0	360	N20W05	1.3	1.5	8:00	...	0.2	0.3
Nov 24	15:10	1245	−3.3	360	N22W07	0.8	1.0	17:00	8.0	1.5	0.095
Nov 25	1:07	2519	−5.0	360	N07E50	10.9	25.5	Nov 26 13:30	15.0	15	0.17
Dec 28	11:30	930	−29.1	360	S10E60	5.0	3.0	19:30	38.5	0.015	0.7
					2001						
Jan 5	16:20	828	−21.2	360	bWL	4.2	2.5	23:00	14.0	0.02	0.3
Jan 20	21:08	1507	−41.1	360	S07E46	6.3	3.5	Jan 21 7:00	9.5	0.004	0.64
Jan 21	19:05	664	−9.7	213	S08E36	0.0	6.5	Jan 22 1:30	35.5	0.03	0.15
Jan 28	15:45	916	3.5	250	S04W59	2.7	1.5	20:00	16.0	0.8	0.42
Feb 11	1:10	1183	−1.7	360	N24W57	2.3	1.5	5:00	15.0	0.009	0.14
Feb 26	4:50	851	8.1	152	bWL	2.6	2.5	10:00	14.0	0.008	0.33
Mar 10	3:30	819	−23.2	81	N27W42	7.0	3.5	14:00	9.0	0.002	0.22
Mar 24	20:08	906	42.9	360	N15E22	18.9	3.0	Mar 25 18:00	18.0	0.001	0.21
Mar 26	13:15	541	4.8	55	N15E27	0.7	5.5	19:30	20.5	0.007	0.26
Mar 29	9:52	942	3.5	360	N14W12	2.1	4.5	16:30	29.5	0.5	1.6
Apr 2	11:00	992	3.0	80	N17W65	1.5	1.5	14:00	...	0.07	2.7
Apr 2	21:43	2505	108.5	244	N19W72	0.8	9.0	Apr 3 7:30	17.5	15	3.4
Apr 9	15:32	1192	1.3	360	S21W04	2.5	1.0	19:00	...	0.1	0.11
Apr 10	5:22	2411	211.6	360	S23W09	3.1	4.5	13:00	23.0	2	0.12
Apr 12	10:10	1184	−20.0	360	S19W43	3.8	2.0	16:00	12.5	0.9	1.3
Apr 15	13:30	1199	−35.9	167	S20W85	0.5	2.5	16:30	11.5	20	0.3
Apr 18	2:10	2465	−9.5	360	bSWL	0.8	4.0	7:00	14.0	5	0.25
Apr 26	11:50	1006	21.1	360	N17W31	4.7	19.5	Apr 27 12:00	14.0	0.02	0.17
May 7	11:55	1223	19.2	205	N26W32	0.6	3.5	16:00	21.5	0.3	0.19
May 20	5:40	546	−0.1	179	bWL	1.3	3.0	10:00	10.0	0.15	0.4
May 29	23:50	2087	−44.5	216	bEL	18.2	46.5	Jun 1 16:30	42.0	0.002	3.1
Jun 4	15:30	464	−2.7	89	N24W59	2.0	0.5	18:00	10.0	0.03	0.31
Jun 15	10:10	1090	9.7	119	S26E41	0.3	...	...	...	0.002	0.39
Jun 15	15:24	1701	56.9	360	bSWL	1.1	1.0	17:30	5.5	0.8	0.51
Jul 11	23:55	736	−8.2	148	S20W65	3.1	8.0	Jul 12 11:00	9.0	0.001	0.22
Jul 19	10:00	1668	−11.6	166	S08W62	5.0	1.0	16:00	21.0	0.0008	0.16
Aug 9	10:20	479	4.4	175	N10W10	7.2	6.5	Aug 10 0:00	...	0.03	0.42
Aug 9	21:05	909	7.2	100	S30E90	9.4	2.5	Aug 10 9:00	6.0	0.2	0.52
Aug 14	10:40	618	−4.8	360	N20W20	5.8	3.5	Aug 14 20:00	15.0	0.01	0.14
Aug 15	23:35	1575	−31.7	360	S20W20[d]	1.4	1.5	Aug 16 2:30	22.5	5	0.3
Sep 12	21:20	668	−0.2	114	S20W75	6.2	1.5	Sep 13 5:00	21.0	0.002	0.17
Sep 15	10:40	478	−4.0	130	S21W49	0.8	2.5	14:00	5.5	0.2	0.041
Sep 17	8:05	1009	−14.5	166	S14E04	9.9	3.0	21:00	21.0	0.003	0.25
Sep 19	5:45	416	−6.1	210	bSWL	4.3	1.5	11:30	23.5	0.004	0.24
Sep 24	10:20	2402	54.1	360	S16E23	1.2	9.5	21:00	21.0	30	0.52
Oct 1	5:30	1405	97.8	360	S18W80	4.5	5.5	15:30	11.5	8	0.27
Oct 9	10:40	973	−41.5	360	S28E08	8.3	0.5	19:30	24.0	0.03	0.14
Oct 19	0:25	558	−25.6	254	N16W18	2.6	2.0	5:00	...	0.09	0.6
Oct 19	16:20	901	−0.7	360	N15W29	1.7	0.5	18:30	...	0.17	0.44
Oct 22	14:50	1336	−8.0	360	S21E18	1.2	3.5	19:30	6.0	0.3	1.2
Nov 4	16:10	1810	−63.4	360	N06W18	1.3	5.5	23:00	25.0	50	0.58
Nov 17	4:50	1379	−22.5	360	S13E42	3.7	20.5	Nov 18 5:00	34.0	0.04	0.22
Nov 22	20:15	1443	−43.3	360	S25W67	0.7	...	...	...	0.5	0.32
Nov 22	22:55	1437	−12.9	360	S17W24	2.6	5.5	Nov 23 7:00	24.5	50	0.21
Dec 11	9:50	891	42.9	121	S25W30	5.7	1.5	17:00	21.0	0.007	0.28
Dec 14	8:50	1506	−21.2	360	N06E90	25.7	16.5	Dec 16 3:00	42.0	0.007	0.42
Dec 26	5:05	1446	−39.9	212	N08W54	0.4	2.5	8:00	12.5	10	0.28
Dec 28	20:05	2216	6.9	360	bSEL	3.9	5.0	Dec 29 5:00	17.0	0.7	0.48

TABLE 1—*Continued*

Date CME (1)	Launch (UT) (2)	v_{CME} (km s^{-1}) (3)	Acceleration (m s^{-2}) (4)	W (deg) (5)	Solar Location[a] (6)	T_O (hr) (7)	T_R (hr) (8)	$\frac{1}{2}$ Peak[b] (UT) (9)	T_D (hr) (10)	20 MeV Peak[c] (11)	O^{+7}/O^{+6} (12)
					2002						
Jan 14.............	5:33	1492	52.3	360	bWL	3.5	20.0	Jan 15 5:00	49.0	0.3	0.2
Jan 27.............	12:10	1136	−19.2	360	bWL	1.8	0.5	14:30	5.0	0.2	0.14
Feb 20	5:55	952	−17.1	360	N12W72	0.6	0.5	7:00	1.5	0.2	0.43
Mar 15...........	22:24	957	−17.4	360	S08W03	3.6	6.0	Mar 16 8:00	23.0	0.015	0.61
Mar 18...........	2:30	989	−2.9	360	S10W25	4.5	20.0	Mar 19 3:00	10.0	0.7	0.5
Mar 22...........	10:53	1750	−22.5	360	bWL	2.6	3.0	16:30	17.5	0.03	0.25
Apr 11	16:00	540	−3.4	70	S15W33	3.0	3.0	22:00	7.0	0.015	0.35
Apr 14	7:25	757	−6.5	76	N19W57	6.6	2.0	16:00	15.5	0.005	0.43
Apr 17	8:00	1240	−19.8	360	S14W34	3.0	4.0	15:00	8.0	0.3	0.21
Apr 21	1:15	2393	−1.4	241	S14W84	0.3	5.5	7:00	26.0	20	2.5
Apr 30	22:44	1103	−2.8	195	bWL	2.8	1.0	May 1 2:30	12.5	0.03	0.22
May 20...........	15:10	553	4.0	35	S21E65	1.8	0.5	17:30	5.0	0.005	0.4
May 22...........	3:22	1557	−10.4	360	S30W34	4.2	13.5	21:00	11.0	1.1	0.56
Jul 7................	10:56	1329	51.6	197	bWL	1.6	3.5	16:00	12.5	0.4	0.26
Jul 9................	17:43	1076	−47.8	360	bSWL	4.8	1.0	23:30	21.5	0.03	0.07
Jul 15.............	19:50	1151	−25.6	360	N19W01	14.2	9.0	Jul 16 19:00	17.0	1	0.88
Aug 3	18:45	1150	−18.8	138	S16W76	3.3	1.0	23:00	5.5	0.004	0.52
Aug 14	1:50	1309	−28.5	133	N09W54	0.7	5.5	8:00	8.5	0.25	0.17
Aug 16	5:53	1378	−3.7	152	N07W83	2.1	0.5	8:30	6.5	0.009	0.14
Aug 16	12:08	1585	−67.1	360	S14E20	4.3	5.5	22:00	26.0	0.03	0.12
Aug 18	21:15	682	1.9	140	S12W19	1.7	0.5	23:30	15.5	0.06	0.25
Aug 20	8:10	1099	−50.1	122	S10W38	0.8	0.5	9:30	8.0	0.025	2.1
Aug 22	1:22	998	−32.8	360	S07W62	1.6	1.0	4:00	16.0	0.4	0.9
Aug 24	0:57	1913	43.7	360	S02W81	1.6	1.0	3:30	21.0	6	0.37
Sep 5	16:32	1748	43.0	360	N09E28	7.5	10.5	Sep 6 10:30	25.5	0.12	0.17
Sep 27	1:08	1502	−61.5	59	SWL	1.3	0.5	3:00	5.0	0.002	0.51
Nov 9	13:10	1838	35.4	360	S12W29	2.3	7.0	22:30	9.0	5.5	1.1
Nov 24	20:00	1077	20.5	360	S17W37	11.0	3.0	Nov 25 10:00	33.5	0.0024	0.16
Dec 19...........	21:25	1092	−36.2	360	N15W09	1.1	1.0	23:30	7.5	0.09	0.13

NOTE.—Table 1 is also available in machine-readable form in the electronic edition of the *Astrophysical Journal*.

[a] Solar source latitude and longitude. bWL and bEL are sources behind the west and east limbs.

[b] The time at which the 20 MeV proton intensity reaches about $\frac{1}{2}$ of peak value. It equals the CME launch time of column (2) + T_O + T_R. Dates are specified for $\frac{1}{2}$ peak UT only where these differ from CME dates given in col. (1).

[c] Peak intensities in photons cm^{-2} s^{-1} sr^{-1} MeV^{-1}, exclusive of shock peaks.

[d] This location was more likely behind the disk near central meridian.

associated solar source regions. We note that the catalog CME parameters are subject to some revision; our parameters were current as of 2004 August.

We determined three characteristic SEP times for each SEP profile. The parameter T_O is the time from CME launch to the onset of the SEP event; T_R is the rise time from the SEP onset to the time at which the intensity was about half of the peak intensity. The purpose here was to determine the time during which most or nearly all of the increase of SEP intensity has occurred, independent of intensity fluctuations around the event peak. Note that the time of half-peak SEP intensity is reached $T_O + T_R$ after the CME launch time. The parameter T_D is the time during which the SEP intensity is within a factor of 2 of the peak value. The time of peak intensity is always taken to be prior to the arrival of any interplanetary shock with an accompanying SEP intensity peak. In some cases T_D is the time only until the beginning of the SEP shock intensity peak. The uncertainties in the SEP onset times, which are determined by eye, are estimated to be about 0.5 hr, and those in T_R and T_D are typically 1 to several hours, depending on the shape of the SEP profile. Examples of SEP events with the SEP times indicated are shown in Figure 1, and the event times are given in columns (7)–(10) of Table 1.

For each CME we used as the launch time the projected time of intersection with 1 $R_\odot$ of the linear best fit to the CME leading-edge height-time plot, shown in the example of Figure 2. As discussed above, fast CMEs have a complex acceleration profile below 2 $R_\odot$, but we must make some simplifying assumption that can be used for a uniform description of CME launches. If we assume that the trajectories of these CMEs are well described by the alternative quadratic height-time fits, then for a typical CME speed of 1200 km s^{-1} and an acceleration of 50 m s^{-2}, we can estimate an uncertainty in the trajectory intersection at 1 $R_\odot$ of ∼0.1 hr; hence, the total uncertainty in T_O is ∼0.6 hr. A 50 minute travel time is required for unscattered 20 MeV protons to traverse 1.2 AU, so a minimum $T_O \sim 0.7$ hr (=50 − 8 minutes) relative to the CME launch would be expected if SEP injection occurred when the CME departed the disk.

2.2. Characteristic Median SEP Times

The full set of 144 SEP events was divided into five groups of longitude range, as shown in Table 2. The characteristic median times for T_O, T_R, and T_D are given there for the full set of 144 SEP events and for each longitude group. For each SEP time we give the probable errors, rounded to the nearest integral hour, within which lie half the data sample (Bevington 1969). Values of T_R and T_D could not be determined for two and nine of the 144 events, respectively, usually because of the presence of an additional SEP event during the rise or duration of the SEP
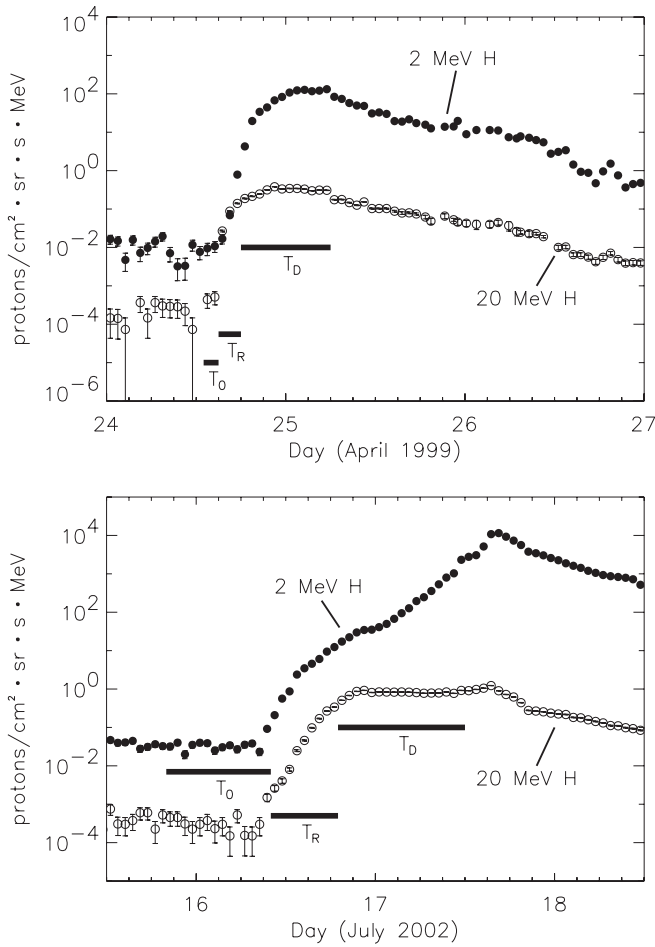
TABLE 2
MEDIAN SEP EVENT TIMES AND PROBABLE ERRORS

Longitude Range	Number	T_O (hr)	T_R (hr)	T_D (hr)
EL-CM	30	4.7^{-3}_{+5}	5.5^{-2}_{+7}	25.0^{-8}_{+11}
W01° to W31°	28	2.4^{-1}_{+2}	2.7^{-1}_{+4}	15.5^{-6}_{+9}
W32° to W62°	29	2.3^{-1}_{+2}	2.0^{+1}_{-1}	11.0^{-3}_{+5}
W65° to W90°	32	1.6^{-1}_{+1}	1.5^{-1}_{+4}	13.2^{-6}_{+8}
Over-WL	25	2.0^{-1}_{+2}	2.5^{-1}_{+2}	14.0^{-7}_{+4}
All Events	144	2.4^{-1}_{+2}	2.5^{-1}_{+3}	15.0^{-7}_{+8}
All ICMEs....................	25–27	2.0^{-1}_{+2}	2.0^{-1}_{+3}	11.5^{-3}_{+10}

profile or because of a data gap. The times are shortest for the well-connected ranges of W32°–W62° and W65°–W90° and longest for the poorly connected east limb to central meridian (EL-CM) range.

2.3. Correlations among SEP Event Characteristics

We looked for correlations among various CME properties and SEP times for the full set and for each of the five longitude groups. The latter step is necessary because of the strong variation in SEP times with solar source longitude. Correlation coefficients r and correlation probabilities (CP; see Table C3 of Bevington 1969) were calculated; the criterion for a significant correlation probability was taken as CP > 0.98.

The peak intensities of the SEP events ranged over 5 decades, from $\sim10^{-3}$ to $\sim10^2$ photons cm^{-2} s^{-1} sr^{-1} MeV^{-1}. It is of interest to know whether the SEP times depend in any way on the SEP peak intensities. We found no correlation of either T_R or T_D with either the peak SEP intensities or with PB, the ratios of peak intensities to the background counting rates. Time T_O declined slightly with increasing peak intensities or PB, but this was due primarily to a number of eastern hemisphere SEP events with long T_O and small peak intensities. We conclude that at most only T_O may be slightly dependent on SEP intensities.

We also looked for correlations among the three SEP times themselves. Since SEP times are generally longer for EL-CM events and shorter for well-connected events, the full set shows a significant correlation between T_O and T_R ($r = 0.46$; CP > 0.999), but no single longitude group shows a significant correlation. Here T_R and T_D are correlated in the full set ($r = 0.49$;

FIG. 1.—*Top*: SEP event of 1999 April 24 showing the periods of the three SEP times T_O, T_R, and T_D for the 20 MeV proton event. The 2 and 20 MeV proton intensity profiles are from the EPACT instrument on the *Wind* spacecraft. The time of the CME launch was determined by extrapolating the linear best-fit height-time profile to 1 $R_\odot$. The event solar origin was over the WL. *Bottom*: Three SEP times for the event of 2002 July 16, which was associated with a CME and a solar flare at N19°W01°. In this case T_D was measured only up to the time of the increase near the shock at ~15:30 UT on July 17.
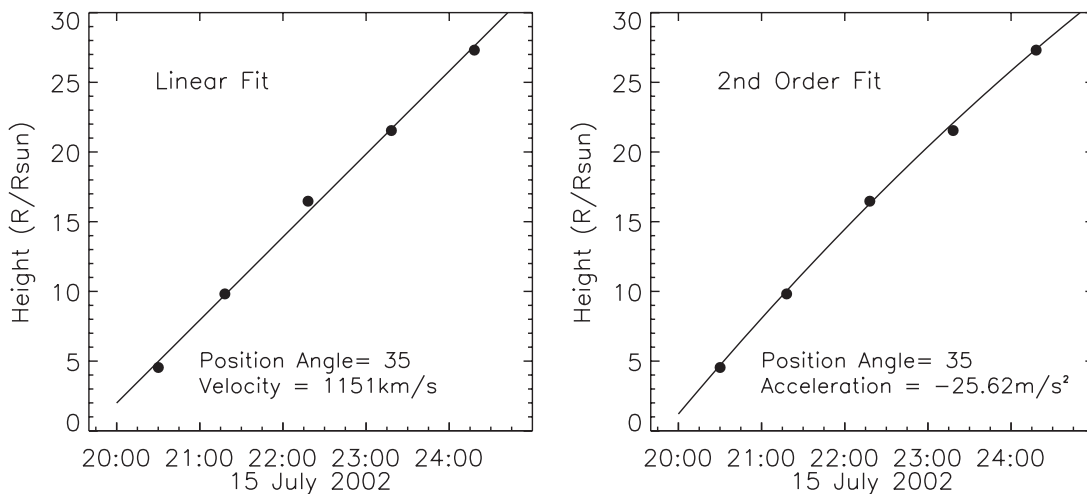
FIG. 2.—*Left*: Linear fit to the height-time plot of the CME associated with the 2002 July 16 SEP event in Fig. 1. The CME launch time was taken to be the time the trajectory of the leading edge intersected 1 $R_\odot$. *Right*: Second-order fit to the CME data with an acceleration of -25.62 m s^{-2}. This figure is reproduced from the LASCO CME Catalog.
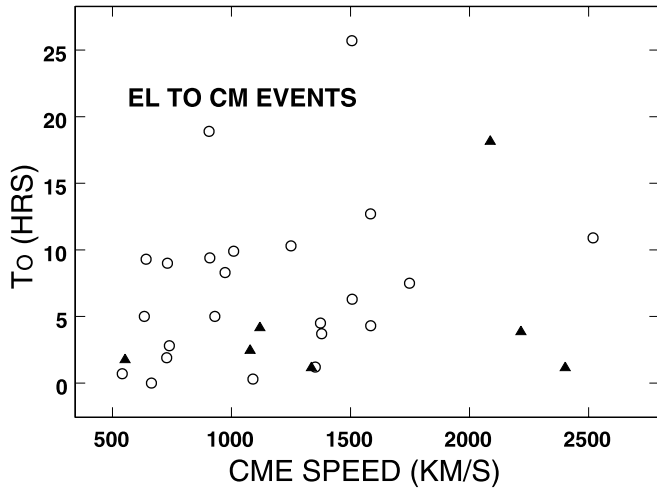
FIG. 3.—SEP onset times T_O vs. CME speeds v_{CME} for the EL-CM events. The two parameters are not correlated. Triangles mark the seven cases when T_O lay within an ICME. These include the two CMEs from behind the east limb, which had speeds of 2087 and 2216 km s^{-1}.

CP > 0.999) and also in the W65°–W90° and the "over west limb" (Over-WL) longitude plots. We conclude that a correlation does exist between T_R and T_D but not between T_O and T_R.

2.4. Correlations between SEP Times and CME Properties

2.4.1. SEP Times and CME Speeds

We find no correlation between T_O and CME speeds v_{CME} for either the full set or any longitude group, such as the EL-CM plot shown in Figure 3. For the full set we find a significant positive correlation ($r = 0.30$; CP > 0.999) of T_R with v_{CME}, but among the longitude groups only the EL-CM and W65°–W90° (Fig. 4) groups show significant correlations. The least-squares best fits indicate an ~0.3 hr increase in T_R for each 100 km s^{-1} increase. The correlations between SEP times and CME properties are given in the form r/CP in Table 3.

The full set also shows a significant correlation ($r = 0.23$; CP = 0.992) of T_D with v_{CME}, but among the longitude groups only the W65°–W90° plot, shown in Figure 5, is also significantly

TABLE 3
CORRELATION COEFFICIENTS AND PROBABILITIES (r/CP)
BETWEEN SEP TIMES AND CMEs

Parameter	T_O	T_R	T_D
EL-CM			
v_{CME}	0.22/0.76	0.43/0.98	0.05/0.20
Acceleration	0.05/0.21	0.09/0.38	0.35/0.93
Width W	0.12/0.46	0.10/0.41	0.28/0.85
O^{+7}/O^{+6}	0.03/0.14	0.26/0.81	0.15/0.56
W01°–31°			
v_{CME}	0.27/0.83	0.04/0.17	0.18/0.58
Acceleration	0.02/0.10	0.06/0.23	0.08/0.27
Width W	0.13/0.49	0.25/0.80	0.14/0.47
O^{+7}/O^{+6}	0.23/0.75	0.19/0.66	0.19/0.61
W32°–62°			
v_{CME}	0.00/0.02	0.26/0.83	0.27/0.84
Acceleration	0.36/0.94	0.12/0.48	0.47/0.99
Width W	0.12/0.47	0.28/0.86	0.39/0.96
O^{+7}/O^{+6}	0.10/0.40	0.14/0.51	0.06/0.23
W65°–90°			
v_{CME}	0.24/0.81	0.48/>0.99	0.53/>0.99
Acceleration	0.06/0.24	0.07/0.28	0.16/0.61
Width W	0.08/0.33	0.36/0.95	0.36/0.95
O^{+7}/O^{+6}	0.32/0.92	0.19/0.69	0.11/0.43
Over-WL			
v_{CME}	0.08/0.31	0.26/0.78	0.18/0.62
Acceleration	0.02/0.06	0.40/0.95	0.30/0.86
Width W	0.07/0.27	0.27/0.80	0.38/0.94
O^{+7}/O^{+6}	0.16/0.55	0.05/0.18	0.14/0.51
All Events			
v_{CME}	0.01/0.12	0.30/>0.99	0.23/>0.99
Acceleration	0.01/0.09	0.04/0.38	0.01/0.14
Width W	0.15/0.92	0.26/>0.99	0.38/>0.99
O^{+7}/O^{+6}	0.01/0.06	0.12/0.86	0.01/0.08

FIG. 4.—SEP rise times T_R vs. CME speeds v_{CME} for the W65°–W90° SEP events. Triangles indicate the nine cases in ICMEs. Here T_R is significantly correlated with v_{CME} with a correlation coefficient of $r = 0.48$.
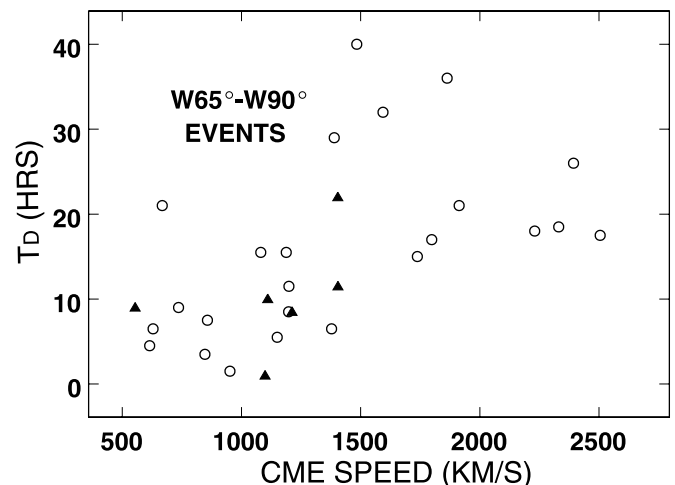

FIG. 5.—SEP duration times T_D vs. CME speeds v_{CME} for the W65°–W90° SEP events. Triangles indicate the six cases in ICMEs. T_D is significantly correlated with v_{CME} with a correlation coefficient of $r = 0.53$.

($r = 0.53$; CP $= 0.998$) correlated. The slopes of the fits indicate an $\sim$1 hr increase in T_D for every 100 km s^{-1} increase in v_{CME}. No attempt was made to correct v_{CME} for longitude effects because of the large angular sizes of these CMEs and because the corrections should have only minimal effect on the correlations, particularly within each longitude group.

2.4.2. *SEP Times and CME Accelerations*

The median acceleration for all 144 CMEs is -6.6 m s^{-2}; 93 are negative and 51 positive in sign. Seven of the 144 CME accelerations were determined from only three data points and therefore perhaps suspect; those seven points were determined not to make a significant difference to the lack of acceleration correlations. The correlation results are definitive: neither the full set nor any longitude group shows a significant correlation with acceleration for either T_O or T_R. We do find one significant correlation for T_D in the W32°–W62° group. In that case T_D increases as the accelerations increase from negative to positive values. However, the EL-CM range show a slightly negative correlation, and for the full set no T_D correlation with acceleration was found.

2.4.3. *SEP Times and CME Widths*

Angular widths W of CMEs associated with SEP events are generally broad (Kahler & Reames 2003). Here $W > 50°$ for all associated CMEs, and half (72 of 144 events) of the associated CMEs are classified as full 360° halo events. We find no correlation of T_O with W, but there is a significant positive correlation ($r = 0.26$; CP $= 0.999$) for the T_R full set. All the T_R longitude groups also show positive correlations, but none is significant. However, the same 360° value for so many CME widths probably diminishes those T_R-W correlations, particularly when only a few CME widths W of a given longitude group are not full halos. We conclude that there is a weak but significant correlation of T_R with W.

As with T_R, a similar significant positive correlation ($r = 0.38$; CP > 0.999) is found for the full T_D set. The T_D longitude groups are all positively correlated with W, but none significantly. To summarize the correlations of SEP times with W, we find no correlation for T_O, but positive correlations for both T_R and T_D, the significance of which may be masked by the large number of halo CMEs.

2.4.4. *SEP Times and Solar Wind Streams and ICMEs*

The SEP times have been compared with the solar wind O^{+7}/O^{+6} ratios measured at the times of SEP onsets by the Solar Wind Ion Composition Spectrometer (SWICS; Gloeckler et al. 1998) experiment on the *Advanced Composition Explorer* (*ACE*) spacecraft. We found no significant correlations for any of the three SEP times versus logs of O^{+7}/O^{+6} in either the full set or any longitudinal group. This indicates that the SEP times are independent of the type of solar wind stream in which they occur.

We have also examined SEP events in which some or all of the SEP times occurred within interplanetary CMEs (ICMEs) determined from solar wind plasma and magnetic field measurements and listed in Table 1 of Cane & Richardson (2003). With the requirement that at least half of a candidate SEP time interval must lie within an ICME interval, we find that 27, 25, and 27 intervals of T_O, T_R, and T_D, respectively, occurred in ICMEs. In the last line of Table 2 we give the median values for the SEP times of all events in ICMEs. Those median SEP times are slightly shorter than the times of all SEP events, but the statistics are too limited to draw firm conclusions about the effects of ICMEs on the SEP times. The most significant effect

appears in the plot of the EL-CM T_O events (Fig. 3), where a number of the short T_O values are associated with ICMEs. In addition, the only two SEP events associated with CMEs from behind the east limb, with CME launches calculated to be 23:50 UT on 2001 May 29 and 20:00 UT on 2001 December 28, both lay within ICMEs.

3. DISCUSSION

We have characterized the distributions of the three SEP times T_O, T_R, and T_D for five solar longitude groups in Table 2. The shorter times found for well-connected SEP events compared with those from the EL-CM or Over-WL groups were anticipated from previous work by van Hollebeke et al. (1975) and by Cane et al. (1988), but they used flare times rather than CME launch times as their basic fiducials. One intriguing basic result is the broad range of each of the three SEP times, even within each longitude group, as can be seen in the example plots of Figures 3–5.

Consistent with the shock model of SEP production are the correlations of T_R and T_D with v_{CME} shown in Figures 4 and 5. The idea is that faster CMEs continue to drive shocks, which then accelerate and inject SEPs for longer times. This result is seen only for the well-connected CMEs and suggests that properties of shocks at CME flanks are less directly coupled to the CME leading edge or nose, the location at which the CME speed profile is determined. We also note that the CME speeds used in this study were measured over many different position angles, and in many cases those angles were not optimal for the field lines connecting the CME shock to the *Wind* spacecraft.

The T_O times of Table 2 allow us to determine the heights of associated CMEs at the times of the initial SEP injections. If we assume scatter-free propagation along a path of 1.2 AU for the first arriving 20 MeV protons and subtract the 8 minute correction for the speed of light, then the SEP onset times at 1 AU should be at least 0.7 hr after solar injection. Subtracting that time from $T_O \sim 1$ to 3 hr of the best-connected events in Table 2 means that the range of heights for a CME with the median v_{CME} of 1100 km s^{-1} is about 3–15 $R_\odot$ when SEP injection begins. The use of the second-order CME speed profiles can shift CME launch times by $\sim$10 minutes, usually to later times since most CME accelerations were negative. These time shifts result in differences of only $\sim$1 $R_\odot$ in CME heights at the times of initial SEP injections. The recent shock models of Li et al. (2003) and Ng et al. (2003) introduce antisunward propagating shocks at 21.5 $R_\odot$ (0.1 AU) and 11.3 $R_\odot$, respectively, since the solar wind structure is too complex for the models at lower heights. The results here suggest that an effort should be made to extend the shock models to lower heights and earlier times to obtain more realistic values of T_O and T_R for their SEP model intensity-time profiles.

We found no dependence of the SEP times on CME accelerations, which were measured in the LASCO C2 and C3 fields of view of 2–30 $R_\odot$. We might ask whether the larger accelerations occurring below 3 $R_\odot$ are significant for the SEP times. Chen & Krall (2003) have determined that the main acceleration of CMEs occurs when the leading edges are below 2–3 $R_\odot$, which is below the initial SEP injection range of 2–15 $R_\odot$ determined above. Thus, the early speed profile, and hence primary acceleration period, does not appear to play a role in the subsequent SEP event times, probably because the SEPs are produced only after shock formation, which takes place after the primary acceleration phase. The peak SEP intensities depend on the CME speeds, so the intensities should therefore indirectly scale with the characteristic initial CME accelerations.

The SEP T_R and T_D are probably correlated with CME widths, but with nearly half the widths reported as $360°$ halos and almost no CMEs with widths less than $50°$, the correlation analysis here is suggestive but not definitive. We might expect that wider, fast CMEs can drive shocks for longer periods of time, resulting in longer injection times for SEPs. Since narrow CMEs are ineffective in shock SEP production (Kahler & Reames 2003), CME width seems to play a significant role in the production of SEP events, but until we have a better way of determining those widths, we cannot quantify that relationship. If CME models, such as the cone model (Zhao et al. 2002; Michalek et al. 2003) are sufficiently accurate to determine intrinsic CME angular widths from the coronagraph observations, then a comparison of SEP times with those angular widths would be useful.

Kahler (2004) found no difference of peak SEP intensities between fast and slow wind streams, and we now find that the SEP times also show no dependence on O^{+7}/O^{+6}, the signature of solar wind speed regimes. If organized solar wind structures such as magnetic clouds serve as confining barriers to the SEPs, then we might expect that T_D of SEPs in MCs would be longer than those SEPs propagating outside MCs. Comparing our SEP events inside ICMEs, of which MCs are a subset, with SEP events in normal solar wind, we found that T_R and T_D for events inside ICMEs are slightly shorter than for events in normal solar wind, although the differences are not statistically significant. We noted in Figure 3, however, that the only two cases in which we associated SEP events with CMEs from behind the east limb involved ICMEs. Cliver et al. (1995) have discussed the problem of extreme propagation of SEPs, in which SEPs appear to be injected as far as $150°$ away from the solar eruptive source region, and presented those SEP events as evidence of widespread coronal shocks. The two CMEs from behind the east limb (Fig. 3) suggest SEP injections into unusual solar magnetic connections (e.g., Richardson & Cane 1996) as the reason for at least some cases of extreme propagation.

REFERENCES

Balch, C. C. 1999, Radiat. Meas., 30, 231

Bevington, P. R. 1969, Data Reduction and Error Analysis for the Physical Sciences (New York: McGraw-Hill)

Bieber, J. W., et al. 2002, ApJ, 567, 622

Brueckner, G. E., et al. 1995, Sol. Phys., 162, 357

Campbell, W. H. 1996, J. Atmos. Terr. Phys., 58, 1171

Cane, H. V., & Erickson, W. C. 2003, J. Geophys. Res., 108, 1203

Cane, H. V., Reames, D. V., & von Rosenvinge, T. T. 1988, J. Geophys. Res., 93, 9555

Cane, H. V., & Richardson, I. G. 2003, J. Geophys. Res., 108, 1156

Chen, J., & Krall, J. 2003, J. Geophys. Res., 108, 1410

Cliver, E. W., Kahler, S. W., Neidig, D. F., Cane, H. V., Richardson, I. G., Kallenrode, M.-B., & Wibberenz, G. 1995, Proc. 24th Int. Cosmic Ray Conf. (Rome), 4, 257

Cliver, E. W., Kahler, S. W., & Reames, D. V. 2004, ApJ, 605, 902

Daibog, E. I., Logachev, Yu.I., Kahler, S., & Kecskemety, K. 2003, Adv. Space Res., 32(12), 2655

Gallagher, P. T., Lawrence, G. R., & Dennis, B. R. 2003, ApJ, 588, L53

Gloeckler, G., et al. 1998, Space Sci. Rev., 86, 497

Gopalswamy, N., Yashiro, S., Kaiser, M. L., Howard, R. A., & Bougeret, J.-L. 2001, J. Geophys. Res., 106, 29219

Gopalswamy, N., Yashiro, S., Lara, A., Kaiser, M. L., Thompson, B. J., Gallagher, P. T., & Howard, R. A. 2003b, Geophys. Res. Lett., 30, 8015

Gopalswamy, N., Yashiro, S., Michalek, G., Kaiser, M. L., Howard, R. A., Leske, R., von Rosenvinge, T., & Reames, D. V. 2003a, in AIP Conf. Proc. 679, Solar Wind Ten, ed. M. Velli et al. (New York: AIP), 608

Kahler, S. W. 1993, J. Geophys. Res., 98, 5607

———. 2001, in Space Weather, ed. P. Song et al. (AGU Geophys. Monogr. 125; Washington: AGU), 109

———. 2003, Adv. Space Sci., 32, 2587

———. 2004, ApJ, 603, 330

Kahler, S. W., McAllister, A. H., & Cane, H. V. 2000, ApJ, 533, 1063

Kahler, S. W., & Reames, D. V. 2003, ApJ, 584, 1063

Kallenrode, M.-B. 2002, J. Atmos. Sol.-Terr. Phys., 64, 1973

Kallenrode, M.-B., & Cliver, E. W. 2001, Proc. 27th Int. Cosmic Ray Conf. (Hamburg), 8, 3314

Klein, K.-L., Chupp, E. L., Trottet, G., Magun, A., Dunphy, P. P., Rieger, E., & Urpo, S. 1999, A&A, 348, 271

Klein, K.-L., & Trottet, G. 2001, Space Sci. Rev., 95, 215

Kocharov, L., Torsti, J., Laitinen, T., & Teittinen, M. 1999, Sol. Phys., 190, 295

Kocharov, L., Torsti, J., St. Cyr, O. C., & Huhtanen, T. 2001, A&A, 370, 1064

Laitinen, T., et al. 2000, A&A, 360, 729

Li, G., Zank, G. P., & Rice, W. K. M. 2003, J. Geophys. Res., 108, 10

Mewaldt, R. A., et al. 2003, Proc. 28th Int. Cosmic Ray Conf. (Japan), 6, 3229

Michalek, G., Gopalswamy, N., & Yashiro, S. 2003, ApJ, 584, 472

Miroshnichenko, L. I., De Koning, C. A., & Perez-Enriquez, R. 2000, Space Sci. Rev., 91, 615

Moon, Y.-J., Choe, G. S., Wang, H., Park, Y. D., Gopalswamy, N., Yang, G., & Yashiro, S. 2002, ApJ, 581, 694

Ng, C. K., Reames, D. V., & Tylka, A. J. 1999, Geophys. Res. Lett., 26, 2145

———. 2003, ApJ, 591, 461

Reames, D. V. 1999, Space Sci. Rev., 90, 413

Reames, D. V., Barbier, L. M., & Ng, C. K. 1996, ApJ, 466, 473

Reames, D. V., Kahler, S. W., & Ng, C. K. 1997, ApJ, 491, 414

Rice, W. K. M., Zank, G. P., & Li, G. 2003, J. Geophys. Res., 108, 5

Richardson, I. G., & Cane, H. V. 1996, J. Geophys. Res., 101, 27521

Shanmugaraju, A., Moon, Y.-J., Dryer, M., & Umapathy, S. 2003, Sol. Phys., 215, 185

Sheeley, N. R., Jr., Hakala, W. N., & Wang, Y.-M. 2000, J. Geophys. Res., 105, 5081

Sheeley, N. R., Jr., Walters, J. H., Wang, Y.-M., & Howard, R. A. 1999, J. Geophys. Res., 104, 24739

St. Cyr, O. C., et al. 2000, J. Geophys. Res., 105, 18169

Stolpovskii, V. G., Daibog, E. I., Kahler, S. W., & Erdos, G. 1998, Adv. Space Res., 21, 543

Tan, L. C., Mason, G. M., Lee, M. A., Klecker, B., & Ipavich, F. M. 1992, J. Geophys. Res., 97, 1597

Torsti, J., Kocharov, L., Innes, D. E., Laivola, J., & Sahla, T. 2001, A&A, 365, 198

Torsti, J., Kocharov, L. G., Teittinen, M., & Thompson, B. J. 1999a, ApJ, 510, 460

Torsti, J., Kocharov, L. G., Vainio, R., Anttila, A., & Kovaltsov, G. A. 1996, Sol. Phys., 166, 135

Torsti, J., Riihonen, E., & Kocharov, L. 2004, ApJ, 600, L83

Torsti, J., et al. 1999b, J. Geophys. Res., 104, 9903

Tylka, A. J. 2001, J. Geophys. Res., 106, 25333

Tylka, A. J., Cohen, C. M. S., Dietrich, W. F., Lee, M. A., Maclennan, C. G., Mewaldt, R. A., Ng, C. K., & Reames, D. V. 2005, ApJ, 625, 474

van Hollebeke, M. A. I., Ma Sung, L. S., & McDonald, F. B. 1975, Sol. Phys., 41, 189

Vashenyuk, E. V., Miroshnichenko, L. I., Sorokin, M. O., Perez-Peraza, J., & Callegos-Kruz, A. 1994, Geomagn. Aeron., 33, 569

von Rosenvinge, T. T., et al. 1995, Space Sci. Rev., 71, 155

Vourlidas, A., Wu, S. T., Wang, A. H., Subramanian, P., & Howard, R. A. 2003, ApJ, 598, 1392

Yago, K., & Kamide, Y. 2003, Space Weather, 1, 1004

Yashiro, S., Gopalswamy, N., Michalek, G., St. Cyr, O. C., Plunkett, S. P., Rich, N. B., & Howard, R. A. 2004, J. Geophys. Res., 109, 7105

Zank, G. P., Rice, W. K. M., & Wu, C. C. 2000, J. Geophys. Res., 105, 25079

Zhang, J., Dere, K. P., Howard, R. A., Kundu, M. R., & White, S. M. 2001, ApJ, 559, 452

Zhao, X. P., Plunkett, S. P., & Liu, W. 2002, J. Geophys. Res., 107, 13